

## Article

# 2-Chloro-4,6-bis{(E)-3-methoxy-4-[(4-methoxybenzyl)oxy]styryl}pyrimidine: Synthesis, Spectroscopic and Computational Evaluation

Otávio Augusto Chaves <sup>1</sup>, Vitor Sueth-Santiago <sup>2,3,†</sup>, Douglas Chaves de Alcântara Pinto <sup>2</sup>, José Carlos Netto-Ferreira <sup>2,4</sup>, Debora Decote-Ricardo <sup>5</sup> and Marco Edilson Freire de Lima <sup>2,\*</sup>

<sup>1</sup> Centro de Química de Coimbra (CQC), Departamento de Química, Universidade de Coimbra, Rua Larga, 3004-545 Coimbra, Portugal; otavioaugustochaves@gmail.com

<sup>2</sup> Departamento de Química Orgânica, Instituto de Química, Universidade Federal Rural do Rio de Janeiro, Seropédica 23890-000, Brazil; vitor\_sueth@hotmail.co.uk (V.S.-S.); douglasdoti@hotmail.com (D.C.d.A.P.); jcnetto@ufrj.br (J.C.N.-F.)

<sup>3</sup> Instituto Federal de Educação, Ciência e Tecnologia do Rio de Janeiro, Campus São Gonçalo, Rua José Augusto Pereira dos Santos, São Gonçalo 24425-004, Brazil

<sup>4</sup> Departamento de Química Orgânica, Instituto de Química, Universidade Federal do Rio de Janeiro, Centro de Tecnologia, Bloco A, Cidade Universitária, Rio de Janeiro 21941-909, Brazil

<sup>5</sup> Departamento de Microbiologia e Imunologia Veterinária, Instituto de Veterinária, Universidade Federal Rural do Rio de Janeiro, Seropédica 23890-000, Brazil; decotecard@ufrj.br

\* Correspondence: marcoedilson@gmail.com

† This work is dedicated to the memory of the honorable Brazilian scientist, teacher, friend and human being Vitor Sueth-Santiago (1987–2021). A victim from COVID-19.



**Citation:** Chaves, O.A.; Sueth-Santiago, V.; Pinto, D.C.d.A.; Netto-Ferreira, J.C.; Decote-Ricardo, D.; Lima, M.E.F.d. 2-Chloro-4,6-bis{(E)-3-methoxy-4-[(4-methoxybenzyl)oxy]styryl}pyrimidine: Synthesis, Spectroscopic and Computational Evaluation. *Molbank* **2021**, *2021*, M1276. <https://doi.org/10.3390/M1276>

Academic Editor: Giovanni Ribaudou

Received: 31 July 2021

Accepted: 29 August 2021

Published: 7 September 2021

**Publisher's Note:** MDPI stays neutral with regard to jurisdictional claims in published maps and institutional affiliations.



**Copyright:** © 2021 by the authors. Licensee MDPI, Basel, Switzerland. This article is an open access article distributed under the terms and conditions of the Creative Commons Attribution (CC BY) license (<https://creativecommons.org/licenses/by/4.0/>).

**Abstract:** A novel curcumin analog namely 2-chloro-4,6-bis{(E)-3-methoxy-4-[(4-methoxybenzyl)oxy]styryl}pyrimidine (compound **7**) was synthesized by three-step reaction. The condensation reaction of protected vanillin with 2-chloro-4,6-dimethylpyrimidine (**6**) was the most efficient step, resulting in a total yield of 72%. The characterization of compound **7** was performed by <sup>1</sup>H and <sup>13</sup>C nuclear magnetic resonance (NMR), as well as high-resolution mass spectrometry. The experimental spectrometric data were compared with the theoretical spectra obtained by the density functional theory (DFT) method, showing a perfect match between them. UV-visible spectroscopy and steady-state fluorescence emission studies were performed for compound **7** in solvents of different polarities and the results were correlated with DFT calculations. Compound **7** showed a solvatochromism effect presenting higher molar extinction coefficient (log ε = 4.57) and fluorescence quantum yield (φ = 0.38) in toluene than in acetonitrile or methanol. The simulation of both frontier molecular orbitals (FMOs) and molecular electrostatic potential (MEP) suggested that the experimental spectra profile in toluene was not interfered by a possible charge transfer. These results are an indication of a low probability of compound **7** in reacting with unsaturated phospholipids in future applications as a fluorescent dye in biological systems.

**Keywords:** curcumin analog; organic synthesis; photophysical properties; steady-state fluorescence; DFT calculation

## 1. Introduction

Turmeric, obtained from the dried rhizomes of *Curcuma longa* (Zingiberaceae), is a golden colored material, commonly used around the world for seasoning and food coloring. Since antiquity, turmeric has been widely used in the treatment of several diseases in traditional Chinese and Indian medicine (traditionally known as Ayurveda, e.g., for the treatment of inflammatory diseases) [1–3]. Curcumin ((1E,6E)-1,7-bis(4-hydroxy-3-methoxyphenyl)hepta-1,6-diene-3,5-dione) also known as diferuloylmethane, is the main chemical component of turmeric (accounting for up to 70%), belonging to the class of diarylheptanoid

metabolites. This compound is mainly responsible for both biological, metal chelator, flavoring, reactivity and pigment properties of turmeric (Figure 1A) [1,4]. Furthermore, curcumin stems present potent antioxidant, anti-inflammatory and anticancer activity due to their capacity to suppress the proliferation of a wide variety of tumor cells and regulate the expression of different enzymes [5]. Some structural modifications in the curcumin moiety based on structure-activity relationship have improved its drug profile (Figure 1). As an example, dimethoxycurcumin showed potential trypanocidal properties with a half-maximal inhibitory concentration ( $IC_{50}$ ) value of 11.07  $\mu$ M [6], while 1-methyl-3,5-bis[(*E*)-4-pyridyl]methylidene]-4-piperidone and 1-isopropyl-3,5-bis[(pyridine-3-yl) methylene] piperidin-4-one showed potential anticancer properties with  $IC_{50}$  values in the 0.7–1.0  $\mu$ M range for H3122 cells lines (lung cancer cell lines) [7]. In addition, a series of asymmetric dihydrothiopyran curcumin analogs demonstrated high inhibition at a submicromolar level against acute promyelocytic leukemia cells [8], and integrating a tetrahydro-4-pyrone linker into curcumin structure led to cell growth inhibition, promoted apoptosis and enhanced irinotecan sensitivity against gastric cancer cells [9]. Finally, theoretical evaluation for some curcumin derivatives (replacing methoxyl groups in the aromatic moieties for bromo, chloro or hydroxyl groups) indicated these novel derivatives as potential inhibitors of amyloid- $\beta$  peptides aggregation in the human brain ( $A\beta$ s—aggregation process involved in the onset of Alzheimer's disease) [10].

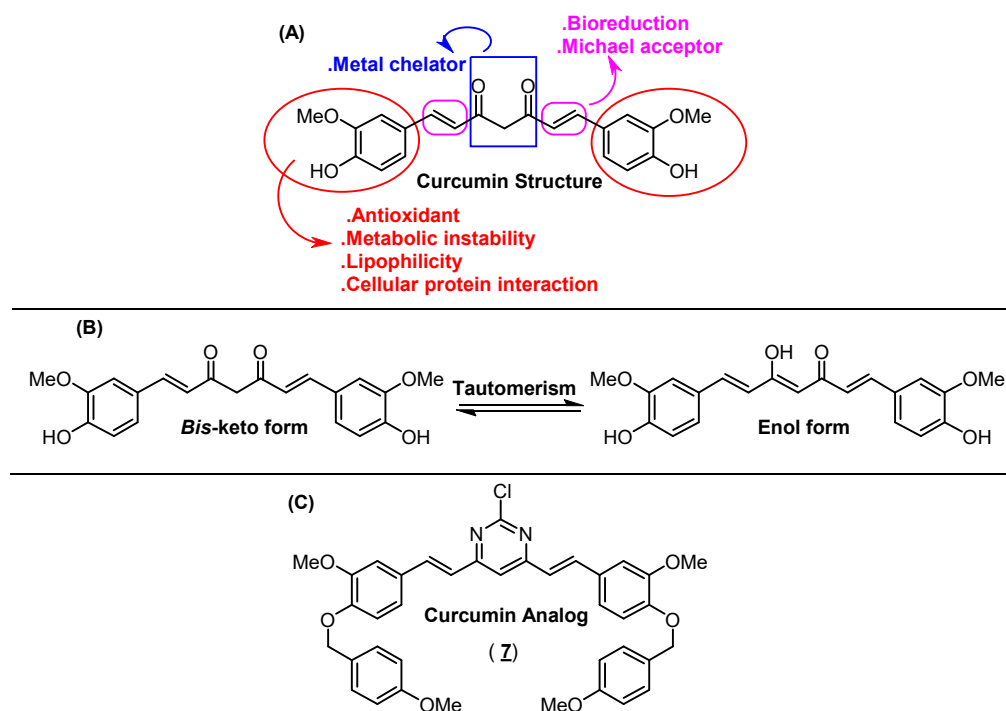
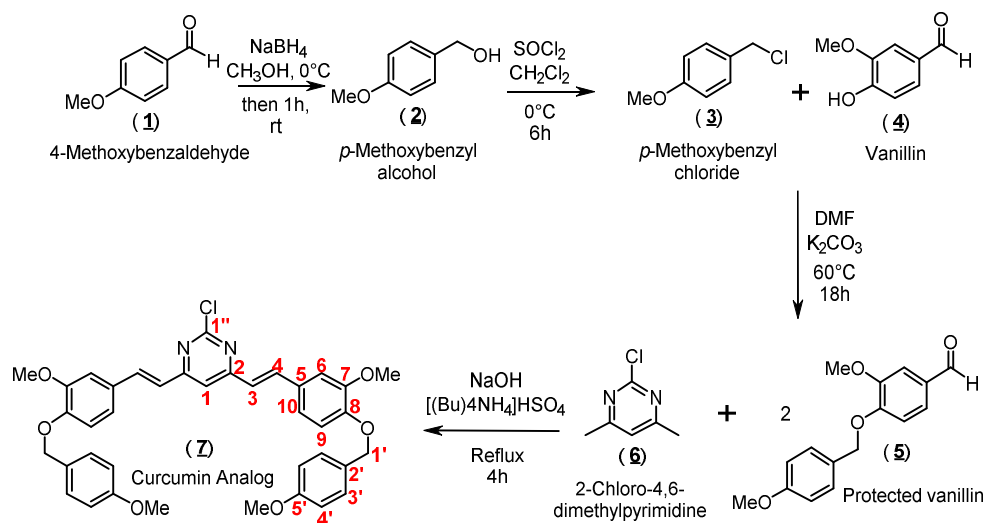


**Figure 1.** (A) Chemical structure of curcumin and its simplified structural-activity relationship. (B) Tautomerism form for curcumin. (C) Chemical structure for the curcumin analog under study—compound 7.

From a structural point of view, the *ortho*-methoxy phenolic groups are symmetrically connected to a seven-carbon chain through an  $\alpha,\beta$ -unsaturated  $\beta$ -diketone group. All these connections will result in a highly conjugated structure that shows UV-visible absorption in the 200–500 nm range, depending on the solvent polarity; however, the spectral properties of curcumin are related to the tautomeric forms (*bis*-keto or enol—Figure 1B) [11]. For this reason, curcumin has been widely explored in terms of spectroscopic properties, showing maximum absorption in the 408–430 nm range in different organic solvents; however, its maximum steady-state fluorescence emission (460–560 nm) is more sensitive than absorption to the solvent polarity, presenting Stokes' shift varying from 2000 to 6000  $cm^{-1}$ .

Furthermore, curcumin shows a low fluorescence quantum yield in most of the solvents, which is significantly reduced in the presence of water [12]. In this sense, novel organic and inorganic compounds based on curcumin moiety have been proposed to improve the photophysical behavior, e.g., curcumin boron complexes can act as a near-infrared imaging fluorescent probe [13], chemical sensor [14] and larger second-order nonlinear property [15].

Based on the background described above on the biological and photophysical importance of curcumin and both its derivatives and analogs, the main goal of the present work is the synthesis of a novel symmetric curcumin analog, namely 2-chloro-4,6-bis((*E*)-3-methoxy-4-[(4-methoxybenzyl)oxy]-styryl)pyrimidine (compound 7—number according to the synthetic steps shown in Scheme 1) (Figure 1C). Its characterization via high-resolution mass spectrometry (HRMS) and experimental or computational Nuclear Magnetic Resonance spectra (NMR— $^1\text{H}$  and  $^{13}\text{C}$ ) will follow the synthetic procedure. The preliminary spectroscopic characterization of compound 7 was also described by UV-visible and steady-state fluorescence techniques for three different solvents (methanol, acetonitrile or toluene), combined with computational results based on Density Functional Theory (DFT) calculations.



**Scheme 1.** Synthetic procedure to obtain the curcumin analog 7.

## 2. Results and Discussion

### 2.1. Organic Synthesis and Structure Determination

The organic synthesis of compound 7 (curcumin analog) was performed through three main steps, as shown in Scheme 1. Basically, the first step was aimed at preparing para-methoxybenzyl chloride (3), which was employed in the derivatization of vanillin (4). Protected vanillin, namely 3-methoxy-4-[(4-methoxybenzyl)oxy]benzaldehyde (5), was then condensed with 2-chloro-4,6-dimethylpyrimidine (6) based on a protocol from Lee and coworkers [16], resulting in the formation of the target compound 7.

Compound 7 was characterized by experimental and computational  $^1\text{H}$ - and  $^{13}\text{C}$ -NMR (Figures S1, S2 and Table S1 in the Supplementary Material), as well as by high resolution mass spectrometry (HRMS). As can be seen in Figure S1 and Table S1, the experimental  $^1\text{H}$ -NMR signals ( $\delta$ ) at 2.50 and 3.30 correspond to DMSO- $d_6$  (solvent) and remnants hydration molecules, respectively, while  $\delta$  at 3.77 and 3.85 correspond to the hydrogens for the methoxy groups connected to  $\text{C}_{5'}$  and  $\text{C}_7$ , respectively. In addition, the signals ( $\delta$ ) in the 6.96–7.89 range were assigned to the hydrogens of the aromatic moiety of compound 7 (details in Figure S1). On the other hand, the experimental  $^{13}\text{C}$ -NMR  $\delta$  (via Distorsionless Enhancement by Polarization Transfer Including the Detection of Quaternary Nuclei—DEPTQ—Figure S2 and Table S1), revealed absorptions compatible with the proposed structure, e.g.,  $\delta$  at 55.58 and 56.09 corresponding to the carbon from the methoxyl groups connected to  $\text{C}_{5'}$  and  $\text{C}_7$ , respectively. In addition,  $\delta$  in the 111.00–166.28 range can be assigned to the carbons present in the aromatic moiety (details in Figure S2) of

compound 7. Overall, the proposed structure for 7 is in agreement with the experimental NMR data described in the literature for a similar compound: (E,E)-4,6-bis-(40-hydroxy-30-methoxystyryl)pyrimidine [16]. To further confirm the structure for compound 7, HRMS experiments revealed the value of  $m/z$  650.2184  $[M]^+$  which is in full agreement with the chemical formula  $C_{38}H_{35}ClN_2O_6$  (calculated monoisotopic mass: 650.2184 g/mol).

Through the rise of reliable quantum chemical computational methods, such as Density Functional Theory (DFT), the DFT-NMR spectra of different organic compounds have been extensively reported. A comparison between the experimental and theoretical spectra in most cases reveals that they show the same profile [17–19]. Figures S1B and S2B show the theoretical DFT spectra ( $^1H$ - and  $^{13}C$ -NMR) for the compound 7 and Table S1 compares the  $\delta_{exp}$  and  $\delta_{calc}$  values (experimental and theoretical, respectively). An inspection of the experimental and theoretical  $\delta$  values revealed that they are practically the same in both cases. As an example, the methyl protons from methoxyl group in  $C_{5'}$ -OCH<sub>3</sub> presented  $\delta_{calc}$  3.77/ $\delta_{exp}$  3.67 and  $\delta_{calc}$  55.58/ $\delta_{exp}$  54.00 for  $^1H$ - and  $^{13}C$ -NMR, respectively. These results are clear indication that the chemical structure of the synthesized compound 7 is in accordance with the proposed structure. In addition, it was also shown that DFT is a good method to simulate NMR spectra for this curcumin analog.

## 2.2. Spectroscopic Study: UV-Vis Absorption and Steady-State Fluorescence Emission

In general, organic compounds based on curcumin are dyes whose structure allows them to be classified as donor-acceptor-donor species (D-A-D) due to the presence of electron donor groups at both ends of the conjugated  $\pi$  system and an electron acceptor group at their central portion [20]. The synthetic compound under study, i.e., compound 7, also shows a D-A-D structure (Figure 2A), with a large absorption band in about 380, 390 and 395 nm in methanol, acetonitrile and toluene, respectively (Figure 2B and Table 1). These bands are probably due to a  $n-\pi^*$  electronic transition, with an additional absorption at low wavelength (<325 nm), corresponding to a  $\pi-\pi^*$  electronic transition in both methanol and acetonitrile [21]. It is important to note that toluene has a cut-off band of about 285 nm. Therefore, for toluene, only maximum absorption bands at 300 and 395 nm were considered. The absorption spectrum in each solvent (Figure 2B) shows a broad band in the high absorption wavelength region (325–450 nm range). The absence of shoulders in the absorption band in this region probably indicates that compound 7 does not present isomeric forms in the ground-state, which is in accordance with the proposed structure (Figure 1C). These results are in opposition to those described for curcumin, which show keto-enol tautomerism (Figure 1B) [22]. A considerable change in the energy of electronic transition in the 325–450 nm range can also be observed (Figure 2B) due to a solvatochromism effect, starting from a polar protic solvent (methanol) to a nonpolar solvent (toluene). For methanol, the presence of a blue shift in the maximum absorption band at 380 nm can be clearly observed, which is probably due to interactions by hydrogen bonding between the solvent and the electron acceptor groups (alkoxyl and the nitrogen atoms of the pyrimidine ring) present in compound 7 [12,22]. In addition, compound 7 showed a higher extinction coefficient ( $\log \epsilon$  at  $\lambda_{max}$  = 380, 390 and 395 nm for methanol, acetonitrile and toluene, respectively—Figure 2C and Table 1) in nonpolar and polar aprotic solvents (e.g.,  $\log \epsilon$  = 4.57 in toluene), a spectroscopic behavior that is very suitable for photosensitizer and fluorescent dyes [12]. These results are similar to those reported in the literature for photosensitizers and fluorescent synthetic diacetoxyboron complexes, also based on curcumin structure [20].

**Table 1.** Photophysical results for the compound 7 in three different solvent polarities.

Solvent <sup>a</sup>	$\lambda_{max}$ (nm)	$\log \epsilon$ <sup>b</sup>	$\lambda_{exc}$ (nm)	$\lambda_{em}$ (nm)	$\Phi_F$	Stokes Shift (nm)	Dimer Formation
Methanol	220; 275; 380	4.19	222; 300; 392	507	0.09	115	No
Acetonitrile	225; 255; 390	4.48	225; 295; 395	504	0.23	109	No
Toluene	300; 395	4.57	304; 396	443	0.38	47	No

<sup>a</sup> UV-cutoff for methanol, acetonitrile and toluene: 210, 190 and 285 nm, respectively [23]. <sup>b</sup> Corresponding to the highest wavelength UV absorption ( $\lambda_{max}$  = 380, 390 and 395 nm for methanol, acetonitrile and toluene, respectively).

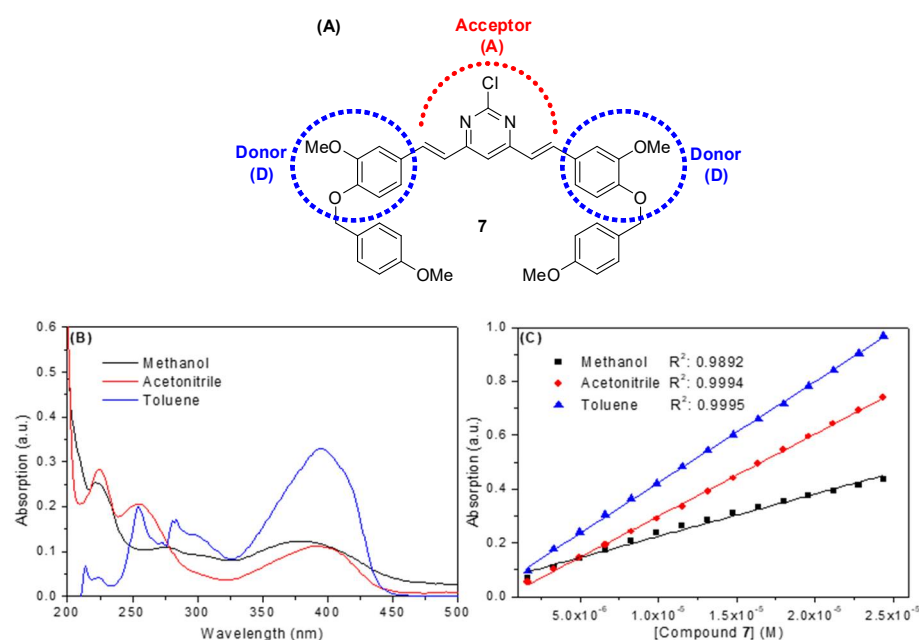


**Figure 2.** (A) Chemical structure of the compound 7 highlighting the D-A-D moieties. (B) UV-visible spectra for the compound 7 in methanol, acetonitrile and toluene.  $[7] = 2.32 \times 10^{-6}$  mol/L (C) Beer-Lambert plots for the determination of  $\epsilon$  value for 7 in three different solvents (at  $\lambda_{\max} = 380, 390$  and  $395$  for methanol, acetonitrile and toluene, respectively).  $[7] = 0.17\text{--}2.44 \times 10^{-5}$  mol/L.

Steady-state fluorescence measurement is a comprehensive approach used to assess the excited state behavior of organic dyes in the presence of metallic species or solvents [20]. As can be seen in Figure 3A and Table 1, compound 7 shows maximum fluorescence emission in methanol, acetonitrile and toluene at 507, 504 and 443 nm, respectively ( $\lambda_{\text{exc}} = 390$  nm, a wavelength in which none of these solvents contribute for the absorption phenomenon). By inspecting the spectra shown in Figure 3A, a significant red shift in the maximum fluorescence emission of compound 7 can be observed when the polarity of the solvent is varied. Thus, for toluene, a non-polar solvent, the maximum fluorescence emission for compound 7 was recorded at 443 nm. In contrast, for the polar solvents methanol or acetonitrile, maximum values were observed at 507 and 504 nm, respectively. The maximum fluorescence emission did not change significantly when using polar protic (methanol) or non-protic solvent (acetonitrile). Thus, it can be concluded that the process of solvation of the lowest energy unoccupied molecular orbital (LUMO) does not involve hydrogen bonding. Further confirmation of these results was made using computational calculations, which showed similar values, for both LUMO ( $-2.41$  and  $-2.31$  eV) and  $|\Delta E|$  ( $3.29$  and  $3.27$  eV) in methanol and acetonitrile, respectively (Table 2). These values justify the similarity between the spectroscopic data obtained in these two solvents. Surprisingly, compound 7 showed LUMO and  $|\Delta E|$  values ( $-2.25$  and  $3.34$  eV, respectively—Table 2) in toluene comparable in magnitude to those calculated for methanol and acetonitrile. However, the maximum fluorescence emission in the former solvent showed a significant blue-shift compared to that observed in the two later solvents (Figure 3).

**Table 2.** Comparison between experimental and theoretical (calculated—DFT) signals ( $\delta$ ) for <sup>1</sup>H- and <sup>13</sup>C-NMR to the compound 7.

Solvent	$\mu$ (D)	$E_{\text{HOMO}}$ (eV)	$E_{\text{LUMO}}$ (eV)	$ \Delta E $ (eV)
Methanol	6.26	$-5.70$	$-2.41$	3.29
Acetonitrile	6.21	$-5.58$	$-2.31$	3.27
Toluene	5.46	$-5.59$	$-2.25$	3.34

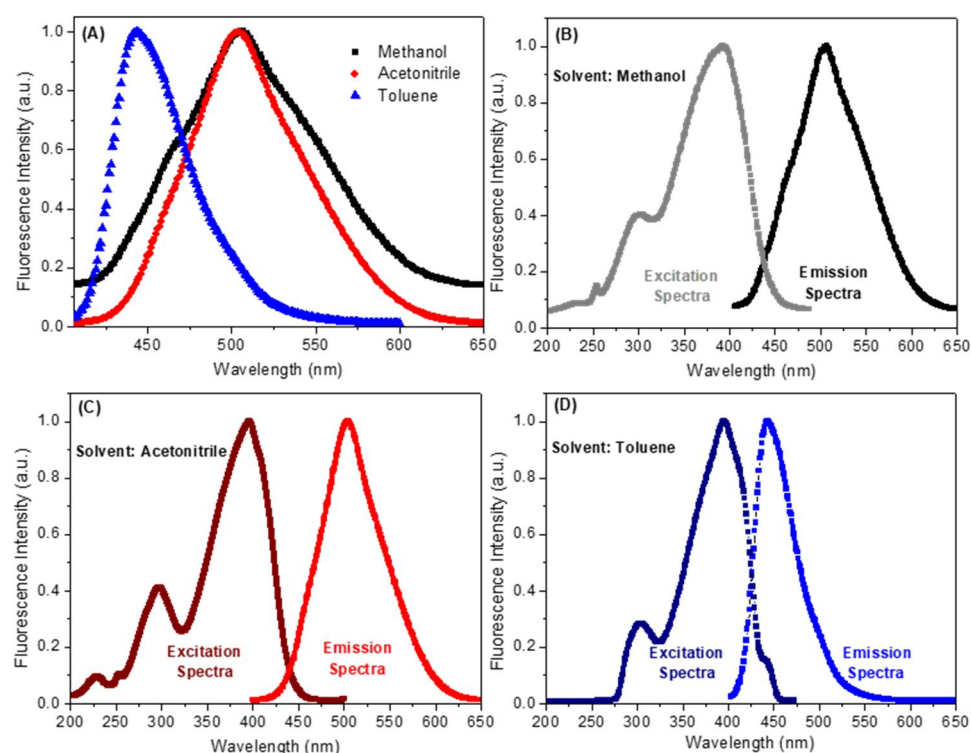


**Figure 3.** (A) Normalized steady-state fluorescence emission spectra for the compound **7** in three different solvents ( $\lambda_{\text{exc}} = 390$  nm and  $[7] = 2.32 \times 10^{-6}$  mol/L). (B–D) Normalized steady-state and excitation spectra for the compound **7** in methanol, acetonitrile and toluene, respectively.

The fluorescence quantum yield ( $\Phi_F$ ) for compound **7** was recorded in methanol, acetonitrile and toluene. All  $\Phi_F$  determinations were performed using  $\lambda_{\text{exc}} = 390$  nm for air saturated samples, with its value varying according to the polarity of the solvent. Compound **7** in methanol presented an extremely low fluorescence quantum yield ( $\Phi_F = 0.09$ ) when compared to acetonitrile ( $\Phi_F = 0.23$ ) and toluene ( $\Phi_F = 0.38$ ) (Table 1), suggesting that its singlet excited state in methanol must be deactivated mainly by a non-radiative process. The excitation spectrum for compound **7** (Figure 3B–D) showed a broadband in the 325–450 nm range, which can be attributed to the  $S_0$ – $S_1$  transition due to its fully superimposed to the corresponding UV–vis absorption spectrum (Figure 2) [22]. In addition, the excitation spectrum in all three solvents is the specular image of the corresponding fluorescence emission spectrum. The Stokes shift reflected the difference between the spectral position at the maximum for the excitation spectrum and the fluorescence emission, dependent on the fluorophore and the solvation environment. The maximum fluorescence emission for compound **7** in methanol, acetonitrile and toluene showed Stokes's shift of 115, 109 and 47 nm, respectively. These results agree with the computational ones, which indicated that more polar solvents typically lead to larger Stokes shifts [24].

In general, dye molecules with a large change in their permanent dipolar moment ( $\mu$ ) exhibit a strong solvatochromism after excitation [22,25]. As shown above, spectroscopic studies for compound **7**, regarding ground-state absorption and steady-state fluorescence emission indicated a different behavior depending on the solvent polarity. Thus, while the absorption spectrum for compound **7** showed a blue shift when the solvent polarity changed from non-polar to polar, a red shift was observed in the case of fluorescence emission spectrum (inverted solvatochromism). These results indicated that there must be a significant change in the dipole moment value ( $\mu$ ) for compound **7**, according to the polarity of the solvent [25]. To gain further insights into the behavior of the dipole moment for compound **7** in the presence of solvents of different polarities, the theoretical values for  $\mu$  were calculated using the DFT method (Table 2). From these calculations, a significant change in the  $\mu$  value was observed from methanol (6.26 D) to toluene (5.46 D). On the

other hand, the  $\mu$  value was quite similar in methanol and acetonitrile (6.26 to 6.21 D, respectively), also justifying the position of the maximum fluorescence in these two solvents, which was red-shifted when compared to toluene. The same solvatochromic profile for curcumin has already been reported [22]; however, these effects are mainly related to the keto-enol equilibrium, which is not the case for compound 7, whose structure does not allow the existence of such equilibrium.

It is known that curcumin at a relatively high concentration can form dimers through a cycloaddition reaction due to its enolic form, in which a C=C double bond is present. This phenomenon directly affects the biological, photophysical and spectral profile of curcumin [26,27]. Even though the structure of compound 7 cannot lead to the formation of dimers due to the impossibility of the presence of an enolic form, it is important to theoretically assess its possible reactivity concerning the occurrence of a charge transfer process between compound 7 and model compounds that have an aromatic ring. The knowledge of this reactivity can help to understand the spectral profile discussed above when using toluene as a non-polar solvent.

The highest occupied molecular orbital (HOMO) and the lowest unoccupied molecular orbital (LUMO) are the most important frontier molecular orbitals (FMOs), playing a crucial role in understanding the stability and chemical reactivity of different compounds. In general, FMOs are responsible for predicting interactions between molecules (e.g., the interaction between small compounds and phospholipids in biological systems), electronic spectra and chemical reactions, such as the dimers' formation [28]. Theoretical studies on the curcumin reaction using FMOs indicated the contribution of HOMO and LUMO from the *o*-methoxyphenol and unsaturated  $\beta$ -diketone groups, respectively [26]. Figure 4A shows the theoretical FMOs representation (DFT method) for compound 7 in methanol, acetonitrile and toluene. The HOMO density for compound 7 is delocalized through the ortho-methoxyphenol portion and the  $\alpha,\beta$ -unsaturated pyrimidine base. It was not found any evidence for the HOMO density delocalized over the oxygen connected to the aromatic group, which is probably due to the presence of the vanillin protected by the para-methoxybenzyl group. On the other hand, the LUMO density is located mainly in the  $\alpha,\beta$ -unsaturated group linked to the pyrimidine ring [28]. Even though the LUMO density is in a possible reactive fraction of compound 7, the fact that this region does not have reactive groups (as an example, a carbonyl group), in association with the presence of the protected vanillin, also affected the localized HOMO density. These results indicated that compound 7 has a low probability of reaction, including a charge transfer process in the presence of toluene.

An alternative that allows examining the reactive behavior of a molecule and can be used to understand the charge transfer process between a target compound and solvents, is the molecular electrostatic potential (MEP) map. The MEP is generated in space around a molecule by charge distribution, especially useful in understanding the sites for electrophilic attack and nucleophilic reactions in the study of biological recognition processes, hydrogen bonding interactions and dimer formation [28,29]. The prediction of the reactive molecular sites via MEP was obtained for compound 7 in the ground and excited singlet states ( $S_0$  and  $S_1$  states, respectively) by applying the DFT method in methanol, acetonitrile and toluene. Figure 4B shows the MEP maps with negative regions (assigned in red), corresponding to sites prone to electrophilic attack, and positive regions (assigned in blue) corresponding to nucleophilic reactivity. These computational results suggested that the possible sites for nucleophilic attack are found around the chlorine atom. However, this negative region is diluted in the  $\alpha,\beta$ -unsaturated system both in the ground-state and excited singlet state, indicating a low possibility of reacting with other compounds, including charge transfer interaction, corroborating the FMOs' results. Overall, the computational results suggested low reactivity, which indicated that compound 7 probably would not react with unsaturated phospholipids in possible applications as a fluorescent dye in biological systems. Furthermore, these results also indicated a low probability of charge transfer between compound 7 and toluene, which cannot be responsible for the spectral

profile for this compound in toluene [26]. In addition, the comparison between the MEP map and the Mulliken charge (Table 3) for the optimized  $S_0$  and  $S_1$  states revealed small changes in the distribution of the associated electronic charge in the ground and excited single states (only for the p-methoxyphenyl moiety). A slight increase was observed in the positive regions of the p-methoxyphenyl moiety; however, it is less rich in electrons when compared to the chlorine atom. These results suggested the pyrimidine ring contributes to the photophysical characteristics of compound 7 and the protected vanillin groups at its extremity can be responsible for possible further effects [30]. The fact that Mulliken's charge in the ground and excited states for compound 7 are practically the same when toluene is used as a solvent reinforced the low probability of charge transfer between this compound and non-polar aromatic solvents.

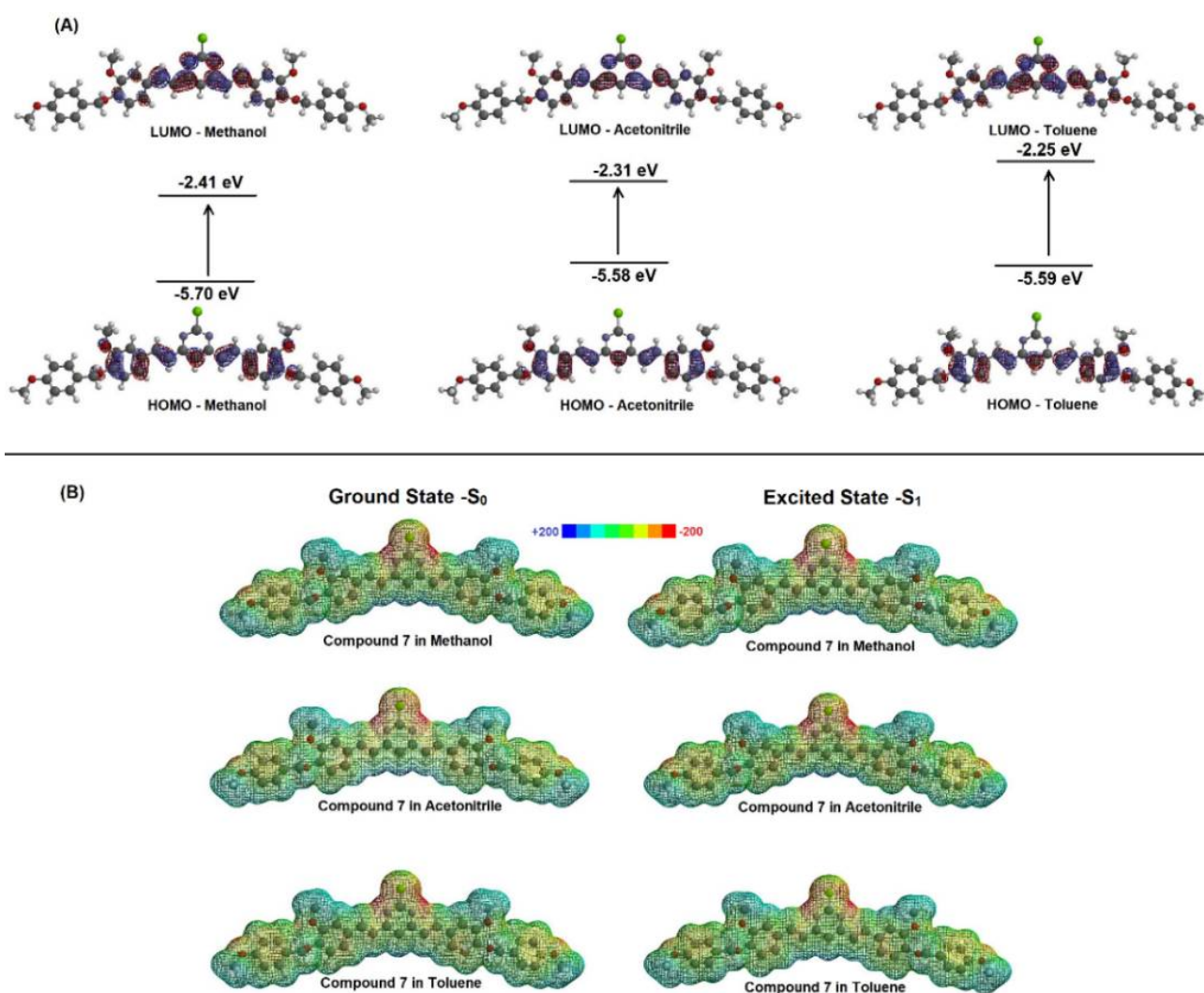


**Figure 4.** (A) HOMO-LUMO density for the compound 7 in methanol, acetonitrile and toluene. (B) Molecular electrostatic potential (MEP) map for the compound 7 (in a.u.) in three different solvents.

**Table 3.** Mulliken charge values for the compound 7 in both ground and excited state.

Position <sup>a</sup>	Mulliken Charge in the Ground State			Mulliken Charge in the Excited State		
	Methanol	Acetonitrile	Toluene	Methanol	Acetonitrile	Toluene
1	−0.194	−0.203	−0.218	−0.194	−0.203	−0.218
2	0.236	0.234	0.285	0.236	0.234	0.285
3	−0.185	−0.189	−0.192	−0.185	−0.189	−0.192
4	−0.193	−0.197	−0.185	−0.193	−0.197	−0.185
5	0.163	0.158	0.172	0.163	0.158	0.172
6	−0.270	−0.279	−0.281	−0.270	−0.279	−0.281
7	0.357	0.372	0.365	0.357	0.372	0.365
8	0.278	0.302	0.317	0.278	0.302	0.317
9	−0.189	−0.201	−0.190	−0.189	−0.201	−0.190
10	−0.184	−0.191	−0.193	−0.184	−0.191	−0.193
1'	−0.126	−0.116	−0.116	−0.126	−0.116	−0.116
2'	0.126	0.131	0.137	0.128	0.132	0.139
3'	−0.185	−0.182	−0.174	−0.182	−0.181	−0.174
4'	−0.198	−0.205	−0.190	−0.198	−0.205	−0.190
5'	0.351	0.376	0.380	0.351	0.376	0.382
6'	−0.198	−0.207	−0.190	−0.196	−0.206	−0.189
7'	−0.211	−0.220	−0.209	−0.210	−0.218	−0.207
1''	0.272	0.270	0.261	0.272	0.270	0.261
C <sub>7</sub> -OCH <sub>3</sub>	−0.242	−0.242	−0.232	−0.242	−0.242	−0.232
C <sub>5'</sub> -OCH <sub>3</sub>	−0.242	−0.240	−0.229	−0.242	−0.240	−0.229

<sup>a</sup> Carbon numeration according to denomination presented in Scheme 1.

### 3. Materials and Methods

All reagents and solvents were purchased from commercial sources (Tedia Ltda, Rio de Janeiro, Brazil and Sigma-Aldrich, Saint Louis, MO, USA) and used without further purification. The Nuclear Magnetic Resonance (NMR) spectra were recorded on a Bruker Ultrashield Plus Spectrometer (Bruker BioSpin GmbH, Rheinstetten, Germany) operating at 500 and 125 MHz for <sup>1</sup>H and <sup>13</sup>C (DEPTQ), respectively, with tetramethyl silane (TMS) as internal reference and deuterated dimethyl sulfoxide (DMSO-d<sub>6</sub>) as solvent (signals for DMSO-d<sub>6</sub>: δ 2.50 and 39.7 for <sup>1</sup>H and <sup>13</sup>C-NMR, respectively). Chemical shifts (δ) were reported in ppm and the coupling constants (*J*) in Hertz [Hz]. The High-Resolution Mass Spectrometry (HRMS) analyses were taken in the positive ion mode under electrospray ionization (ESI) method on a Bruker 9.4 T Apex-Qh (FT-ICR) (Bruker Daltonik GmbH Life Sciences, Bremen, Germany). Reactions were monitored by Thin Layer Chromatography (TLC) on Merck silica gel 60 F245 aluminum sheets and TLC spots were visualized by inspection of the plates under ultraviolet (UV) light (254 and 365 nm).

#### 3.1. Synthesis of 2-Chloro-4,6-bis(*E*)-3-methoxy-4-[(4-methoxybenzyl)oxy]-styryl}pyrimidine (Compound 7)

The organic synthesis of compound 7 was performed through three main steps: Firstly, synthesis of compound 3 was accomplished by reducing 1.80 mL of 4-methoxybenzaldehyde (1) (1.15 mmol) by sodium borohydride (NaBH<sub>4</sub>). Initially, 0.28 g (7.5 mmol) of NaBH<sub>4</sub> was slowly added to a solution of (1) in 50 mL of methanol at 0 °C. The resulting solution (4-methoxybenzaldehyde + NaBH<sub>4</sub> in methanol) was left under stirring at room temperature for 1 h. The reaction was stopped by the addition of 50 mL of distilled water. The product was extracted with ethyl ether (3 × 50 mL) and the combined organic phases were washed with saturated sodium chloride solution (2 × 50 mL) and dried over anhydrous sodium sulfate (Na<sub>2</sub>SO<sub>4</sub>). The solvent was removed under reduced pressure without heating. A white solid (para-methoxybenzyl alcohol, 2) was formed, which was then dissolved in 30 mL of dry dichloromethane (CH<sub>2</sub>Cl<sub>2</sub>) and cooled in an ice bath. Then, 1.5 mL of thionyl chloride (SOCl<sub>2</sub>, 2.46 g, 20 mmol) was added dropwise to replace the hydroxyl group in 2 with a chlorine atom, a better leaving group for the second step of the reaction. The formed mixture was kept under a dry nitrogen atmosphere. Upon completion

of the reaction, the solvent and excess  $\text{SOCl}_2$  were removed by evaporation under reduced pressure. The crude product was isolated as a colorless oil with a quantitative yield and characterized by mass spectrometry (MS/MS:  $m/z$  158  $[\text{M} + 2]^+$ ; 156  $[\text{M}]^+$ ; 121; 77; 51).

In the second synthetic step, in a bottom flask, compound **3** was solubilized in 30 mL of dry dimethylformamide (DMF), to which 2.20 g of vanillin (**4**, 15 mmol in DMF) and oven-dried potassium carbonate ( $\text{K}_2\text{CO}_3$ ; 2.40 g, 18 mmol) were added. To remove the produced acid gas (HCl) without the entrance of atmospheric air, the flask containing the resulting suspension was coupled to a glass flowmeter and maintained at ambient pressure under stirring for 18 h. Then, the reaction mixture was poured into crushed ice, yielding a white crystalline solid corresponding to compound **5**, which was filtered and recrystallized from ethyl acetate. The yield (83%) was calculated from the initial amount of **1** used in the previous step, and compound **5** was characterized by mass spectrometry (MS/MS:  $m/z$  272  $[\text{M}]^+$ ; 121; 77).

Finally, in the last step, 4 mmol of the protected vanillin (**5**) were condensed with 2 mmol of 2-chloro-4,6-dimethylpyrimidine (**6**) under 20 mL of an aqueous sodium hydroxide solution (NaOH, 4 mol/L) containing 0.29 mmol of tetrabutylammonium bisulfate ( $[(\text{Bu})_4\text{NH}_4] \text{HSO}_4$ ). This step was based on a protocol from Lee and coworkers [16]. The reaction mixture was refluxed until the formation of a yellow gum, which was then filtered and recrystallized from ethyl acetate, yielding a yellow solid (yield of 72% for the target compound **7**).  $^1\text{H-NMR}$  (500 MHz,  $\text{DMSO-d}_6$ )  $\delta$  (ppm): 7.87 (d, 2H,  $J = 16.0$  Hz); 7.61 (s, 1H); 7.40 (m, 6H); 7.27 (d, 2H,  $J = 5.0$  Hz); 7.20 (d, 2H,  $J = 16.0$  Hz); 7.12 (d, 2H,  $J = 5.0$  Hz); 6.96 (d, 4H,  $J = 7.0$  Hz); 5.07 (s, 4H); 3.95 (s, 6H); and 3.77 (s, 6H).  $^{13}\text{C-NMR}$  DEPTQ (125 MHz,  $\text{DMSO-d}_6$ )  $\delta$  (ppm): 166.2 (C1''); 160.8 (C2); 159.5 (C5'); 150.1 (C8); 149.8 (C7); 138.7 (C4); 130.1 (C3'); 129.1 (C5); 128.6 (C2'); 123.1 (C3); 122.6 (C10); 114.9 (C6); 114.3 (C4'), 113.7 (C9); 111.0 (C1); 70.1 (C1'); 56.1 (C7-OCH<sub>3</sub>); 55.6 (C5'-OCH<sub>3</sub>). HRMS  $m/z$  650.2184.

### 3.2. Spectroscopic Measurements

The UV-Vis spectra were measured in a Shimadzu model Mini 1240 (Shimadzu Scientific Instruments, Kyoto, Japan) at room temperature (ca 298 K). In a quartz cell (1.0 cm optical path), 3 mL of methanol, acetonitrile or toluene was used as solvent to measure the UV-spectra of compound **7** (concentration of  $2.32 \times 10^{-6}$  mol/L) in the 200–500 nm range. The molar extinction coefficient ( $\epsilon$ ) for compound **7** in the three different solvents (methanol, acetonitrile or toluene) was calculated using Beer-Lambert law (Equation (1)):

$$A = \epsilon \cdot l \cdot c \quad (1)$$

where  $l$ ,  $A$  and  $c$  are the cuvette cell pathlength, absorbance and molar concentration of the compound **7** ( $0.17$ – $2.44 \times 10^{-5}$  mol/L), respectively.

Steady-state fluorescence spectra measurements were performed using an optical spectrometer Jasco J-815 (Jasco Easton, MD, USA). A thermostated cuvette holder Jasco PFD-425S15F (Jasco Easton, MD, USA) was employed to control the temperature in the quartz cell (1.0 cm optical path). All spectra were recorded as the average of three scans with appropriate background corrections. The steady-state fluorescence spectrum of the compound **7** (concentration of  $2.32 \times 10^{-6}$  mol/L) in methanol, acetonitrile or toluene was obtained in the 406–650 nm range ( $\lambda_{\text{exc}} = 390$  nm). The corresponding excitation spectrum was recorded at  $\lambda_{\text{em}} = 507$ , 504 and 443 nm in methanol, acetonitrile, and toluene, respectively. The evaluation of the aggregation process was carried out by recording the steady-state fluorescence spectrum upon successive additions of the compound **7** in the concentration range of  $0.17$ – $2.44 \times 10^{-5}$  mol/L in all three different solvents (data shown only for acetonitrile). The fluorescence quantum yield ( $\phi$ ) at 298 K was calculated using Equation (2) and anthracene as a reference ( $\lambda_{\text{exc}} = 390$  nm) [31]:

$$\phi = \phi_{\text{ref}} \cdot \frac{I_{\text{sample}}}{I_{\text{ref}}} \cdot \frac{A_{\text{ref}}^{390\text{nm}}}{A_{\text{sample}}^{390\text{nm}}} \cdot \frac{n^2}{n_{\text{ref}}^2} \quad (2)$$

where  $\phi_{ref}$ ,  $I$ ,  $A^{390nm}$  and  $n^2$  are the quantum yield for the reference compound (anthracene) [32], integral of the steady-state fluorescence emission spectra, absorbance at 390 nm (0.070 a.u.) and refractive index of the solvent, respectively. The subscript “ref” denotes the respective parameters for the reference compound (anthracene).

#### 4. Conclusions

The curcumin analog 2-chloro-4,6-bis((*E*)-3-methoxy-4-[(4-methoxybenzyl)oxy]-styryl)pyrimidine (compound 7) was synthesized by three-step reaction. Basically, the first step was aimed at preparing *para*-methoxybenzyl chloride, which was employed in the derivatization of vanillin. Protected vanillin, namely 3-methoxy-4-((4-methoxybenzyl)oxy)benzaldehyde, was then condensed with 2-chloro-4,6-dimethylpyrimidine resulting in the formation of the target compound 7 with a final yield of 72%. The experimental and theoretical (DFT) signals of compound 7 by  $^1\text{H}$  and  $^{13}\text{C}$ -NMR confirmed the proposed structure, reinforced by HRMS  $m/z$  650.2184  $[\text{M}]^+$  for  $\text{C}_{38}\text{H}_{35}\text{ClN}_2\text{O}_6$ . Compound 7 showed a large absorption band in about 380, 390 and 395 nm in methanol, acetonitrile and toluene, respectively, while steady-state fluorescence emission of compound 7 showed a solvatochromism effect with higher fluorescence quantum yield ( $\phi = 0.38$ ) in toluene than in acetonitrile or methanol. The FMOs and MEP results indicated the absence of a possible charge transfer when toluene was used as solvent. Overall, the results indicated a low probability of compound 7 reacting with unsaturated phospholipids for future applications as a fluorescent dye in biological systems.

**Supplementary Materials:** The following are available online, Figures S1 and S2: The experimental and theoretical (DFT)  $^1\text{H}$ - and  $^{13}\text{C}$ -NMR spectra for the compound 7. Table S1: Comparison between experimental and theoretical (calculated-DFT) signals ( $\delta$ ) for  $^1\text{H}$ - and  $^{13}\text{C}$ -NMR to the compound 7.

**Author Contributions:** Conceptualization, M.E.F.d.L. and O.A.C.; synthesis and molecule characterization, V.S.-S., D.C.d.A.P. and M.E.F.d.L.; spectroscopic analysis and computational calculations, O.A.C. and J.C.N.-F.; writing—original draft preparation, O.A.C., V.S.-S. and M.E.F.d.L.; writing—review and editing, J.C.N.-F., M.E.F.d.L. and D.D.-R. All authors have read and agreed to the published version of the manuscript.

**Funding:** This research was funded by the Brazilian agencies: Coordenação de Aperfeiçoamento de Pessoal de Nível Superior (CAPES), Conselho Nacional de Desenvolvimento Científico e Tecnológico (CNPq) and Fundação Carlos Chagas Filho de Amparo à Pesquisa do Estado do Rio de Janeiro (FAPERJ). The funders had no role in the design of the study; in the collection, analyses or interpretation of data; in the writing of the manuscript or in the decision to publish the results.

**Institutional Review Board Statement:** Not applicable.

**Informed Consent Statement:** Not applicable.

**Data Availability Statement:** Not applicable.

**Acknowledgments:** The authors acknowledge Professor Nanci Câmara de Lucas Garden from Institute of Chemistry at Universidade Federal do Rio de Janeiro (UFRJ, Brazil) for the spectroscopic facilities. O.A.C. also thanks Fundação para a Ciência e a Tecnologia (FCT—Portuguese Foundation for Science and Technology) for the PhD fellowship 2020.07504.BD.

**Conflicts of Interest:** The authors declare no conflict of interest.

#### References

1. Sueth-Santiago, V.; Mendes-Silva, G.P.; Decoté-Ricardo, D.; de Lima, M.E.F. Curcumin, the golden powder from turmeric: Insights into chemical and biological activities. *Quím. Nova* **2015**, *38*, 538–552. [[CrossRef](#)]
2. Goel, A.; Kunnumakkara, A.B.; Aggarwal, B.B. Curcumin as “Curecumin”: From kitchen to clinic. *Biochem. Pharm.* **2008**, *75*, 787–809. [[CrossRef](#)]
3. Khor, P.Y.; Aluwi, M.F.F.M.; Rullah, K.; Lam, K.W. Insights on the synthesis of asymmetric curcumin derivatives and their biological activities. *Eur. J. Med. Chem.* **2019**, *183*, 111704. [[CrossRef](#)] [[PubMed](#)]
4. Nelson, K.M.; Dahlin, J.L.; Bisson, J.; Graham, J.; Pauli, G.F.; Walters, M.A. The essential medicinal chemistry of curcumin. *J. Med. Chem.* **2017**, *60*, 1620–1637. [[CrossRef](#)] [[PubMed](#)]

5. Aggarwal, B.B.; Kumar, A.; Bharti, A.C. Anticancer potential of curcumin: Preclinical and clinical studies. *Anticancer Res.* **2003**, *23*, 363–398. [[PubMed](#)]
6. Sueth-Santiago, V.; Moraes, J.B.B.; Alves, E.S.S.; Vannier-Santos, M.A.; Freire-de-Lima, C.G.; Castro, R.N.; Mendes-Silva, G.P.; Del Cistia, C.N.; Magalhães, L.G.; Andricopulo, A.D.; et al. The effectiveness of natural diarylheptanoids against *Trypanosoma cruzi*: Cytotoxicity, ultrastructural alterations and molecular modeling studies. *PLoS ONE* **2016**, *11*, e0162926. [[CrossRef](#)]
7. Bland, A.R.; Bower, R.L.; Nimick, M.; Hawkins, B.C.; Rosengren, R.J.; Ashton, J.C. Cytotoxicity of curcumin derivatives in ALK positive non-small cell lung cancer. *Eur. J. Pharmacol.* **2019**, *865*, 172749. [[CrossRef](#)]
8. Tan, K.L.; Ali, A.; Du, Y.; Fu, H.; Jin, H.X.; Chin, T.M.; Khan, M.; Go, M.L. Synthesis and evaluation of bisbenzylidenedioxotetrahydrothiopyranones as activators of endoplasmic reticulum (ER) stress signaling pathways and apoptotic cell death in acute promyelocytic leukemic cells. *J. Med. Chem.* **2014**, *57*, 5904–5918. [[CrossRef](#)] [[PubMed](#)]
9. Qiu, P.; Zhang, S.; Zhou, Y.; Zhu, M.; Kang, Y.; Chen, D.; Wang, J.; Zhou, P.; Li, W.; Xu, Q.; et al. Synthesis and evaluation of asymmetric curcuminoid analogs as potential anticancer agents that down regulate NF- $\kappa$ B activation and enhance the sensitivity of gastric cancer cell lines to irinotecan chemotherapy. *Eur. J. Med. Chem.* **2017**, *139*, 917–925. [[CrossRef](#)]
10. Shinzato, T.; Sato, R.; Suzuki, K.; Tomioka, S.; Sogawa, H.; Shulga, S.; Blume, Y.; Kurita, N. Proposal of therapeutic curcumin derivatives for Alzheimer's disease based on ab initio molecular simulations. *Chem. Phys. Lett.* **2002**, *738*, 136883. [[CrossRef](#)]
11. Waranyoupalin, R.; Wongnawa, S.; Wongnawa, M.; Pakawatchai, C.; Panichayupakaranant, P.; Sherdshoopongse, P. Studies on complex formation between curcumin and Hg(II) ion by spectrophotometric method: A new approach to overcome peak overlap. *Cent. Eur. J. Chem.* **2009**, *7*, 388–394. [[CrossRef](#)]
12. Priyadarsini, K.I. Photophysics, photochemistry and photobiology of curcumin: Studies from organic solutions, bio-mimetics and living cells. *J. Photochem. Photobiol. C* **2009**, *10*, 81–95. [[CrossRef](#)]
13. Ran, C.; Xu, X.; Raymond, S.B.; Ferrara, B.J.; Neal, K.; Bacskai, B.J.; Medarova, Z.; Moore, A. Design, synthesis, and testing of difluoroboron-derivatized curcumins as near infrared probes for in vivo detection of amyloid- $\beta$  deposits. *J. Am. Chem. Soc.* **2009**, *131*, 15257–15261. [[CrossRef](#)]
14. Chaicham, A.; Kulchat, S.; Tumchareern, G.; Tuntulani, T.; Tomapatanaget, B. Synthesis, photophysical properties, and cyanide detection in aqueous solution of BF<sub>2</sub>-curcumin dyes. *Tetrahedron* **2010**, *66*, 6217–6223. [[CrossRef](#)]
15. Margar, S.N.; Rhyman, L.; Ramasami, P.; Sekar, N. Fluorescent difluoroboron-curcumin analogs: An investigation of the electronic structures and photophysical properties. *Spectrochim. Acta A* **2016**, *152*, 241–251. [[CrossRef](#)] [[PubMed](#)]
16. Lee, Y.S.; Kim, H.Y.; Kim, Y.S.; Seo, J.H.; Roh, E.J.; Han, H.; Shin, K.J. Small molecules that protect against  $\beta$ -amyloid-induced cytotoxicity by inhibiting aggregation of  $\beta$ -amyloid. *Bioorg. Med. Chem.* **2012**, *20*, 4921–4935. [[CrossRef](#)] [[PubMed](#)]
17. Da Silva, H.C.; De Almeida, W.B. Theoretical calculations of <sup>1</sup>H NMR chemical shifts for nitrogenated compounds in chloroform solution. *Chem. Phys.* **2020**, *528*, 110479. [[CrossRef](#)]
18. Soares, B.A.; Firme, C.L.; Maciel, M.A.M.; Kaiser, C.R.; Schilling, E.; Bortoluzzi, A.J. Experimental and NMR theoretical methodology applied to geometric analysis of the bioactive clerodane trans-dehydrocrotonin. *J. Braz. Chem. Soc.* **2014**, *25*, 629–638.
19. Souza, L.G.S.; Almeida, M.C.S.; Lemos, T.L.G.; Ribeiro, P.R.V.; Canuto, K.M.; Braz-Filho, R.; Del Cistia, C.N.; Sant'Anna, C.M.R.; Barreto, F.S.; de Moraes, M.O. Brazoides A-D, New Alkaloids from *Justicia gendarussa* Burm. F. Species. *J. Braz. Chem. Soc.* **2017**, *28*, 1281–1287. [[CrossRef](#)]
20. Lyu, H.; Wang, D.; Cai, L.; Wang, D.-J.; Li, X.-M. Synthesis, photophysical and solvatochromic properties of diacetoxyboron complexes with curcumin derivatives. *Spectrochim. Acta A* **2019**, *220*, 117126. [[CrossRef](#)]
21. Balasubramanian, K. Theoretical calculations on the transition energies of the UV-visible spectra of curcumin pigment in turmeric. *Ind. J. Chem. A* **1991**, *30*, 61–65.
22. Patra, D.; Barakat, C. Synchronous fluorescence spectroscopic study of solvatochromic curcumin dye. *Spectrochim. Acta A* **2011**, *70*, 1034–1041. [[CrossRef](#)]
23. Przybytek, J.T. *High-Purity Solvent Guide*, 1st ed.; Burdick & Jackson Laboratories: Muskegon, MI, USA, 1980.
24. Lakowicz, J.R. ; *Principles of Fluorescence Spectroscopy*, 3rd ed.; Springer: New York, NY, USA, 2006.
25. Jacques, P. On the relative contributions of nonspecific and specific interactions to the unusual solvatochromism of a typical merocyanine dye. *J. Phys. Chem.* **1986**, *90*, 5535–5539. [[CrossRef](#)]
26. Fujisawa, S.; Atsumi, T.; Ishihara, M.; Kadoma, Y. Cytotoxicity, ROS-generation activity and radical-scavenging activity of curcumin and related compounds. *Anticancer Res.* **2004**, *24*, 563–570.
27. Masuda, T.; Toi, Y.; Bando, H.; Maekawa, T.; Takeda, Y.; Yamaguchi, H. Structural identification of new curcumin dimers and their contribution to the antioxidant mechanism of curcumin. *J. Agric. Food Chem.* **2002**, *50*, 2524–2530. [[CrossRef](#)] [[PubMed](#)]
28. Kosar, B.; Albayrak, C. Spectroscopic investigations and quantum chemical computational study of (E)-4-methoxy-2-[(p-tolylimino)methyl]phenol. *Spectrochim. Acta A* **2011**, *78*, 160–167. [[CrossRef](#)]
29. Politzer, P.; Lane, P. A computational study of some nitrofluoromethanes. *Struct. Chem.* **1990**, *1*, 159–164. [[CrossRef](#)]
30. Lisboa, C.S.; de Lucas, N.C.; Garden, S.J. Synthesis of novel substituted methoxybenzo[2,3-b]carbazole derivatives via C-H functionalization. Experimental and theoretical characterization of their photophysical properties. *Dyes Pig.* **2016**, *134*, 618–632. [[CrossRef](#)]
31. Coppo, R.L.; Zanoni, K.P.S.; Iha, N.Y.M. Unraveling the luminescence of new heteroleptic Ir(III) cyclometalated series. *Polyhedron* **2019**, *163*, 161–170. [[CrossRef](#)]
32. Katoh, R.; Suzuki, K.; Furube, A.; Kotani, M.; Tokumaru, K. Fluorescence quantum yield of aromatic hydrocarbon crystals. *J. Phys. Chem. C* **2009**, *113*, 2961–2965. [[CrossRef](#)]